Journal of Materials and Environmental Science
ISSN : 2028-2508
e-ISSN : 2737-890X
CODEN : JMESCN

J. Mater. Environ. Sci., 2026, Volume 17, Issue 2, Page 345-355

http://www.jmaterenvironsci.com

Study of Cadmium Adsorption Isotherms on Mixed Maghemite–Hematite Nanoparticles

Koua Moro [1], Ignace Christian M'Bra [2*], Xavier N'Doua Armel Kessé [3], Aimé Serge Ello[4]

[1]*Département de Mathématiques Physique Chimie, Université Peleforo GON COULIBALY, BP 1328 Korhogo, Côte d'Ivoire.*
[2]*Laboratoire de Thermodynamique et Physico-Chimie du Milieu (LTPCM), Unité de Formation et de Recherche Sciences Fondamentales et Appliquées, Université Nangui ABROGOUA, 02 BP 801 Abidjan 02, Côte d'Ivoire.*
[3]*Unité de Formation et de Recherche Agriculture, Ressources Halieutiques et Agro-Industries (ARHAI), Université de San Pedro, Côte d'Ivoire.*
[4]*Laboratoire de Constitution et Réaction de la Matière (LCRM), Unité de Formation et de Recherche de Sciences des Structures de la Matière et de la technologie, Université Félix Houphouët-Boigny, Côte d'Ivoire.*
**Corresponding author, Email address: mbraignace@yahoo.fr*

Received *28 Nov 2025,*
Revised *19 Fev 2026,*
Accepted *20 Feb 2026*

Keywords:
- ✓ *Cadmium;*
- ✓ *Adsorption*;
- ✓ *Nanoparticles;*
- ✓ *Maghemite;*
- ✓ *Hematite*

Citation*: Koua Moro, Ignace Christian M'Bra, Xavier N'Doua Armel Kessé, Aimé Serge Ello (2026) Study of Cadmium Adsorption Isotherms on Mixed Maghemite–Hematite Nanoparticles, J. Mater. Environ. Sci., 17(2), 345-355*

Abstract: This study investigates the adsorption of cadmium onto iron nanoparticles synthesized via the coprecipitation method. Adsorption is recognized as an effective technique for the removal of pollutants, particularly trace metals such as cadmium, which remain toxic even at low concentrations. Various adsorption isotherm models (including Langmuir, Freundlich, Temkin, Jovanovic, among others) were employed to model the experimental data. The iron nanoparticles were characterized using techniques such as X-ray diffraction (XRD) and transmission electron microscopy (TEM). The results indicate that the sample synthesized with NaOH (NP-Na) exhibited the highest adsorption capacity (19.36 mg/g). The Jovanovic and Langmuir isotherm models demonstrated a strong fit to the experimental data, while the Hill model proved to be the most effective in describing the adsorption phenomenon. These results highlight the importance of nanoparticle properties in the adsorption efficiency of trace metals.

1. Introduction

The migration of polluants in aqueous media and subsequent development of containment measures have resulted in the use of techniques to remove them in aqueous media (Ayawei et *al.* (2005); El Hammari *et al.* (2022). Among various methods developed for purification and separation, the adsorption process has received remarkable attention due to its inexpensive, uncomplicated and eco-friendly nature. IUPAC defines adsorption as "the increase in the concentration of a substance at the interface of a condensed and a liquid or gaseous layer owing to the operation of surface forces" (Calvert (1990). Adsorbate is the substance in the solid, liquid or gas phase, which is adsorbed, and the substance (surface) into which the adsorbate is adsorbed is called adsorbent. Adsorption processes are categorized into physical and chemical classes based on the nature of forces between adsorbate and adsorbent. The

importance of the adsorption process has encouraged researchers from many disciplines to better understand this process. Numerous experimental and theoretical studies (molecular dynamics simulations and density functional theory (DFT) methods) have been conducted for this purpose (Azzaoui et *al*. (2023); Alshahateet et *al*. (2024). Among these various data, the adsorption isotherms and their corresponding equations characterize the adsorption processes in a complete and thorough manner. The adsorption isotherm describes and predicts the amount of adsorbed material as a function of pressure (or concentration) at a constant temperature (Zhuang et *al*. (2020).

In the recent times, linear regression analysis has been one of the most applied tools for defining the best fitting adsorption models because it quantifies the distribution of adsorbates, analyzes the adsorption system, and verifies the consistency of theoretical assumptions of adsorption isotherm model (Faust et *al*. (2013). But, because of the inherent bias created by linearization, several error functions have been used to address this shortfall. Concomitant with the evolution of computer technology, the use of nonlinear isotherm modelling has been extensively used.

Trace metals such as lead, cadmium in the environment area serious threat to plants, animals and even humans because of their bioaccumulation, no biodegradable property and toxicity even at low concentrations (Chowdhury et *al*. (2017). High levels of cadmium exposure (1 $mg.m^{-3}$) may result in several complications leading to death. Recent data also suggest increased cancer risks and increased mortality in environmentally exposed populations (Kazantzis et *al*. (1992). The World Health Organization (WHO) has set a maximum limit of 3 µg L^{-1} Cd in drinking water. Thus, it is necessary to remove the cadmium from the environment and monitor its content in various environment samples. In the present work, mixed maghemite–hematite nanoparticles were synthesized by coprecipitation method with three basic solution NH_4OH, KOH and NaOH. The prepared materials were used for the adsorption of cadmium in an aqueous medium. The study of the cadmium adsorption process on these materials was carried out using nonlinear models of several adsorption isotherms.

2. Methodology

2.1 Synthesis

Iron oxide nanoparticles were synthesised by the co-precipitation method using an aqueous solution of Fe^{2+} and Fe^{3+} with a stoichiometric ratio of 1:2 according to our previous work (Moro et *al*. (2023) ; (Moro et *al*. (2022). The synthesis was done according to the following operating procedure: a mixture of 50 mL of Fe^{2+} and Fe^{3+} previously prepared with adding in 50 mL of deionized water 1.41 g and 2.76 g of $FeSO_4$, $7H_2O$ and $FeCl_3$, $6H_2O$ respectively. We added 180 mL of deionized water under stirring to finally obtain 300 mL. Different quantities corresponding to 4M concentrations of ammonium hydroxide (NH_4OH), sodium hydroxide (NaOH) and potassium hydroxide (KOH) solutions were added stepwise with stirring. The black precipitates obtained between pH 10 and 12, were recovered, washed several times with deionized water until to pH = 7 and then dried at 70 °C overnight. The samples were denoted, respectively as NP-K; NP-Na and NP-NH, where NP indicates nanoparticle and K, Na and NH the precipitating solution KOH NaOH and NH_4OH, used respectively to synthesize iron oxide nanoparticles.

2.2 Characterization

XRD was employed for analyzing the phase of the synthesized iron oxide nanomaterials. The XRD patterns were obtained using a Bruker D8 powder (XRD) instrument employing CuKα radiation (λ =1.5418 Å). The iron oxide nanoparticles were further characterized using a Transmission Electron Microscopy (TEM) by using JOEL JEM-2100F model with a 200 keV. Nitrogen gas adsorption

measurements were performed at -196 °C by using a micrometrics tristar II plus instrument. Before adsorption measurements all samples were outgassed at 200 °C for at least 2 h. The BET (Brunauer–Emmett–Teller) surface area was calculated from nitrogen adsorption isotherms in the relative pressure (p/p_0) range of 0.05-0.20 The total pore volume was estimated from the amount adsorbed at a relative pressure of 0.98 For magnetic measurements, a vibrating sample magnetometer (VSM, Lakeshore, model 7400 series) was used at room temperature. The magnetic response of the iron oxide nanoparticles was also studied using a squid magnetometer (MPMS, Evercool, 7 T Squid instrument supplied by Quantum Design).

2.3 Cadmium adsorption experiments

In order to measure cadmium removal by the synthesized iron oxide nanoparticles, batch adsorption experiments were conducted by mixing 0.1 g of the iron oxide with 25 mL of cadmium solutions in 50 mL at room temperature. Metal solutions from 5 to 50 mg/L were prepared by dissolving $Cd(NO_3)_2$ of deionized water and adjusting the pH to 6.7 corresponding to the optimum pH (maximal adsorption conditions of cadmium) for cadmium metal ions. The iron oxide nanoparticles were added in each solution shaken in a mechanical shaker at 150 rpm for 24 h to achieve equilibrium, and then filtered through a 0.45 µm syringe filter. The residual concentrations of cadmium ions in the aqueous filtrated were measured using atomic absorption spectrophotometer (spectrAA20) to assess the trace metal adsorption capacity. The amount of trace metals adsorbed per unit weight of iron oxide nanoparticles (Qe, mg/g) was calculated using the following **Eqn. 1**:

$$\mathbf{Q_e = \frac{(C_0 - C_e)V}{m}} \qquad \textbf{Eqn. 1}$$

C_0 and C_e represent the initial and equilibrium concentrations (mg/L) of the metal ions (Cd^{2+}) in the solution. V is the aqueous solution volume (L) and m, is the mass (g) of the iron oxide materials.

2.3 Adsorption isotherms

Cadmium adsorption isotherms on iron oxide nanomaterials were grouped according to the number of parameters of the isotherm model. Thus, for models with two parameters, the adsorption isotherms were fitted to nonlinear Temkin, Jovanovic, Langmuir and Freundlich models, which are the most frequently used models for describing sorption isotherms. The Langmuir isotherm model is defined as **Eqn. 2** (Guo et *al*. (2019), while the Freundlich isotherm model is given in **Eqn. 3**. (Walsh et *al*. (2020):

$$\mathbf{Q_e = \frac{abC_e}{1 + bC_e}} \qquad \textbf{Eqn. 2}$$

$$\mathbf{\log Q_e = \frac{\log C_e}{n} + \log k} \qquad \textbf{Eqn. 3}$$

The Temkin and Jovanovic isotherms model are defined respectively as **Eqn.4** (Ayawei et *al.* (2017) and **5** (Al-Ghouti et *al*. (2020):

$$\mathbf{q_e = B \ln(AC_e} \qquad \textbf{Eqn. 4}$$

$$q_e = q_m\left(1 - e^{K_j Ce}\right) \qquad \textbf{Eqn. 5}$$

Qe is the mass of metals adsorbed per mass of iron oxide (mg/g) at equilibrium, while Ce represents the equilibrium concentration (mg/L) of the metals.

The Langmuir constants are **a** and **b** referred to the adsorption capacity and adsorption rate, respectively.
The adsorption constants for the Freundlich model are k and n, the adsorption constants for Temkin are **A** and **B**. Those of Jovanovic are q_m and K_j.
For models with three parameters, the adsorption isotherms of Cd^{2+} on iron oxide nanomaterials were fitted to nonlinear Redlich-Peterson, Toth, Khan, Koble-Corrigan, Radke-Prausnitz, Jossens, Sips, Hill isotherms model. The non-linear equations of these different adsorption isotherms are given respectively by **Eqn. 6** (Hashem et *al*. (2021), 7 (Ayawei et *al*. (2017), 8 (Sivarajasekar et *al*. (2014), 9 (Hashem et *al*. (2021), 10 (Ocampo-Pérez et *al*. (2013), 11 (Walsh et *al*. (2020), **12** and **13** (Ayawei et *al*. (2017) :

$$\mathbf{q_e} = \frac{\mathbf{K_R}.\mathbf{C_e}}{\mathbf{1} + \mathbf{a_R}.\mathbf{C_e}^{\mathbf{g}}} \qquad \textbf{Eqn. 6}$$

Where $\mathbf{q_e}$: quantity of adsorbate adsorbed on the equilibrium adsorbent (mg/g); $\mathbf{K_R}$: Redlich-Peterson isotherm constant (L/g); **g:** the exhibitor between 0 and 1; $\mathbf{a_R}$: Redlich-Peterson constant (L/mg); $\mathbf{C_e}$: equilibrium adsorbate concentration (mg/L):

$$\mathbf{q_e} = \mathbf{q_m}.\frac{\mathbf{K_T C_e}}{(\mathbf{1} + (\mathbf{K_T}.\mathbf{C_e})^{\mathbf{t}})^{\frac{\mathbf{1}}{\mathbf{t}}}} \qquad \textbf{Eqn. 7}$$

where $\mathbf{q_e}$: equilibrium adsorbed quantity (mg/g); $\mathbf{q_m}$:maximum amount of adsorption (L/mg); $\mathbf{C_e}$: equilibrium adsorbate concentration (mg/L); $\mathbf{K_T}$: Toth isotherm constant; **t**: Toth isotherm constant:

$$q_e = \mathbf{q_m}.\frac{\mathbf{K_K}.\mathbf{C_e}}{(\mathbf{1} + \mathbf{K_K}.\mathbf{C_e})^{\mathbf{a_K}}} \qquad \textbf{Eqn. 8}$$

$\mathbf{q_e}$: equilibrium adsorbed quantity (mg/g); $\mathbf{q_m}$:maximum amount of adsorption (L/mg); $\mathbf{K_K}$: Khan isotherm constant; $\mathbf{C_e}$: equilibrium adsorbate concentration (mg/L); $\mathbf{a_K}$: exponent of Khan's model:

$$\mathbf{q_e} = \frac{\mathbf{A_K}.\mathbf{C_e}^{\mathbf{p}}}{(\mathbf{1} + \mathbf{B_K}.\mathbf{C_e}^{\mathbf{p}})} \qquad \textbf{Eqn. 9}$$

Where $\mathbf{q_e}$: equilibrium adsorbed quantity (mg/g); $\mathbf{C_e}$: equilibrium adsorbate concentration (mg/L); $\mathbf{A_K}$ et $\mathbf{B_K}$: Koble-Corrigan isotherm constants; **p**: exposent of Koble-Corrigan's isotherm model:

$$\mathbf{q_e} = \frac{\mathbf{a}.\mathbf{C_e}}{\mathbf{1} + \mathbf{bC_e^B}} \qquad \textbf{Eqn. 10}$$

Where $\mathbf{q_e}$: equilibrium adsorbed quantity (mg/g); $\mathbf{C_e}$: equilibrium adsorbate concentration (mg/L); **a** and **b**: Radke-Prausnitz isotherm constant (L/g); B: exponent of the Radke-Prausnitz isother:

$$\mathbf{q_e} = \frac{\mathbf{K}.\mathbf{C_e}}{\mathbf{1} + \mathbf{J}.\mathbf{C_e}^{\mathbf{n}}} \qquad \textbf{Eqn. 11}$$

Where $\mathbf{q_e}$: equilibrium adsorbed quantity (mg/g); $\mathbf{C_e}$: equilibrium adsorbate concentration (mg/L); **K**: Jossens isotherm constant; **J** : Jossens isotherm constant; **n** : exponent of the Jossens isotherm:

$$q_e = q_m.\frac{(K_S.C_e)^{n_S}}{1 + (K_S.C_e)^{n_S}} \qquad \textbf{Eqn. 12}$$

$\mathbf{q_e}$: equilibrium adsorbed quantity (mg/g); $\mathbf{C_e}$: equilibrium adsorbate concentration (mg/L); $\mathbf{q_m}$: maximum adsorption quantity (mg/g); $\mathbf{K_S}$: Sips isotherm constant (L/g); $\mathbf{n_S}$: exponent of the Sips isotherm:

$$q_e = \frac{q_{SH} \cdot C_e{}^{n_H}}{K_H + C_e{}^{n_H}} \qquad \text{Eqn. 13}$$

$\mathbf{q_e}$: equilibrium adsorbed quantity (mg/g); $\mathbf{C_e}$: equilibrium adsorbate concentration (mg/L); $\mathbf{q_{SH}}$: maximum adsorption quantity (mg/g); $\mathbf{K_H}$: Hill isotherm constant (L/g); $\mathbf{n_H}$: exponent of the Hill isotherm.

3. Results and Discussion

3.1 Characterization of nanoparticles

The results of characterization of nanoparticles are summarized in **Table 1**.

Table 1. Magnetics properties, particle size and results of adsorption measurements.

Adsorbents	Saturation magnetization (emu/g)	Surface area S_{BET} (m^2/g)	Pore volume (cm^3/g)	Size of particles (nm)
NP-NH	75	84	0.210	13.20
NP-K	61	94	0.221	09.17
NP-Na	58	113	0.235	08.00

As shown in **Table 1**, the surface area obtained depends on the precipitation agent used. The NP-NH sample containing maghemite particles therefore showed much larger particle sizes than the maghemite/hematite mixture of the NP-Na, NP-K s samples. Also, the larger the particles, the higher the saturation magnetization. In our previous work, we have shown that strong magnetization leads to agglomeration of particles which causes the increase in size (Moro et *al*. (2022). These results align with findings indicating that saturation magnetization generally increases with particle size until a plateau is reached (Smolensky et *al*. (2013). Some studies have highlighted this correlation, attributing it to factors such as the increasing proportion of bulk-like atoms relative to surface atoms as size increases (Kolhatkar et *al*. (2013) ; (Thapa et *al*. (2004). However, some research has also noted that for very small nanoparticles (less than approximately 10 nm), saturation magnetization may decrease due to the dominance of surface effects (Thapa et *al*. (2004). As observed by Chaitanya Varma et al., variations in saturation magnetization and coercive field can be explained in terms of magnetic anisotropy (Varma et *al*. (2012). The specific characteristics of the material, the synthesis method employed, and the experimental conditions can all influence the observed relationship between particle size and saturation magnetization (Chen et *al*. (2021) .

3.2 Removal of trace metals Cd

Figure 1 illustrates the capacities for the removal of cadmium trace metals across the three samples. The observed adsorption capacities were quantified as 25.26%, 30.45%, and 44.29% for the NP-NH, NP-K, and NP-Na samples, respectively. These findings indicate that the NP-Na sample demonstrates a substantially higher removal efficiency compared to the NP-K sample. Conversely, the NP-NH sample exhibits the lowest capacity for cadmium removal.

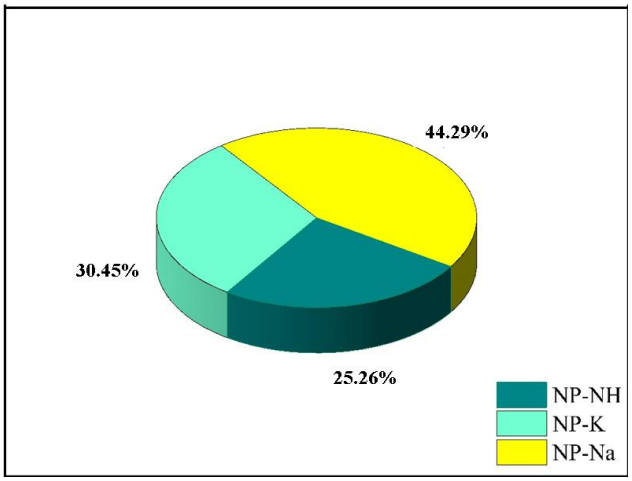

Figure 1. Trace metals removal capacities of synthesized iron oxides

The observed results can be elucidated through the material properties delineated in **Table 1**. As indicated therein, the NP-Na sample exhibits a significantly greater surface area in comparison to the NP-NH and NP-K samples. This augmented capacity for heavy metal adsorption in the NP-Na sample can be attributed to a relatively higher density of micropores and mesopores, which are more prevalent in NP-Na than in its NP-NH and NP-K counterparts, thereby creating conducive conditions for heavy metal retention. Furthermore, the efficacy of heavy metal removal has been demonstrated to be intricately linked to the particle size of iron oxide (Eze et *al.* (2013); a reduction in particle size correlates with an increased specific surface area, enhancing the material's adsorption capacity. Consequently, these findings elucidate the comparatively inferior heavy metal removal performance of the NP-NH and NP-K samples, as noted in previous studies (Liosis et *al.* (2021).

3.3 Isotherms model with two parameters

Figure 2 shows the adsorption isotherms of Langmuir, Freundlich, Temkin and Jovanovic for adsorption of cadmium on ammonium oxides (NH_4OH), sodium (NaOH) and potassium (KOH) by nonlinear analysis. **Table 2** presents the values of the corresponding isotherm parameters, their correlation coefficients (R^2), their reduced correlation coefficients (adjusted R^2) and the reduced chi-square test (χ^2) for each parameter.

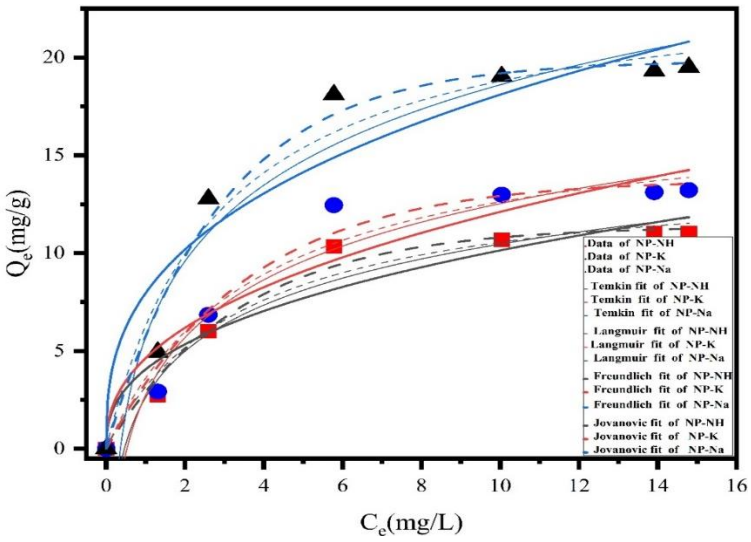

Figure 2. Comparison of the isotherms of Langmuir, Temkin, Freundlich and Jovanovic with the experimental data of NP-Na, NP-K and NP-NH.

Table 2. Parameters for traces metal sorption isotherms fitted with Langmuir and Freundlich for the samples NP-Na, NP-K and NP-NH.

Models	Parameters	Cadmium (Cd)		
		NP-NH	NP-K	NP-Na
Langmuir	q_m (mg/g)	14.25406	17.4707	24.13943
	K_L (L/mg)	0.28548	0.26062	0.35156
	R^2	0.96892	0.96188	0.96435
	Reduced Chi-square (χ^2)	0.77298	1.41021	2.69145
	Adj.R^2	0.9627	0.95425	0.95722
	RSS	3.86489	7.05103	13.45725
Temkin	B (J/mol)	3.40284	4.2527	5.60102
	K_T (L/mg)	2.1637	1,90495	2.77062
	R^2	0.92244	0.91742	0.89431
	Reduced Chi-square (χ^2)	1.16923	1.95512	4.4526
	Adj.R^2	0.90306	0.89678	0.86789
	RSS	4.67693	7.8205	17.81042
Freundlich	K_F (L/mg)	4.05582	4.63112	7.95493
	n_F	2,51238	2,39518	2.80035
	R^2	0.92574	0.91622	0.91783
	Reduced Chi-square (χ^2)	1.84665	3.09898	6.20311
	Adj.R^2	0.91089	0.89946	0.90139
	RSS	9.23327	15.49489	31.01554
Jovanovic	K_J (L/g)	0.29606	0.27957	0.3425
	q_m (mg/g)	11.3898	13.76514	19.83443
	R^2	0.98399	0.97829	0.98065
	Reduced Chi-square (χ^2)	0.39805	0.80311	1.46053
	Adj.R^2	0.98079	0.97395	0.98065
	RSS	1.99025	4.01553	7.30265

In Table 2 and Figure 2, high R^2 are derived by fitting experimental data into the Jovanovic isotherm model ($R^2 > 0.967$) and the Langmuir isotherm model ($R^2 > 0.935$), as compared with the Temkin isotherm model ($R^2 > 0.858$) and Freundlich isotherm model ($R^2 > 0.805$). Meanwhile, the values of standard errors (SE) for each parameter obtained in Freundlich and Temkin isotherms model are

correspondingly higher than that of the other two models. These suggest that both Jovanovic isotherm model and the Langmuir isotherm model can generate a satisfactory fit to the experimental data, while Freundlich and Temkin isotherm model cannot. As shown, the values of maximum adsorption capacity determined using Langmuir model was 14.254; 0.260 and 24.139 mg /g for NP-NH, NP-K and NP-Na respectively. These values are not near the experimental adsorbed amounts and don't correspond to the adsorption isotherm plateau, which indicates that the modelling of Langmuir for the adsorption system is unacceptable. Among these models, the best representation of the experimental results of adsorption isotherms is obtained using the Jovanovic model. According to Table 2, the correlation coefficients (0.95667), adjusted correlation (0.94583) are very good and the reduced Chi-square value (χ^2) which is on average close to 1. Therefore, by comparison, the order of the isotherm best fits the three sets of experimental data in this study is: Jovanovic (Chu et al. (2023) > Langmuir > Temkin > Freundlich.

3.4 Isotherms model with three parameters

Figure 3a. and **3b**. show the adsorption isotherms of Koble-Corrigan, Redlich-Peterson, Jossens, Radke-Prausnitz, Khan, Toth, Sips and Hill. **Table 3** shows the values of the corresponding isotherm parameters. We find that among the three-parameter isotherms of our study, those that are closer to the experimental values are the Hill and Koble-Corrigan isotherms. These give the same values in **Table 2**. Hill and Koble-Corrigan isotherms give correlation coefficients (0.9936), adjusted correlation (0.98933) which are good and the reduced Chi-square value (χ^2) which is on average very low (less than 0.3). This makes it possible to say that the Hill and Koble-Corrigan models fit better to the experimental data than the two parameters cited (Jovanovic model). We classify these isothermal models from the most fitted to the experimental data at least. We noticed a superimposition of some isotherms; notably the Redlich-Peterson, Toth and Radke-Prausnitz isotherms. This has been translated into the symbol (>). It says :

Koble-Corrigan Hill > Redlich-Peterson Radke-Prausnitz Toth > Jossens > Khan > Sips.

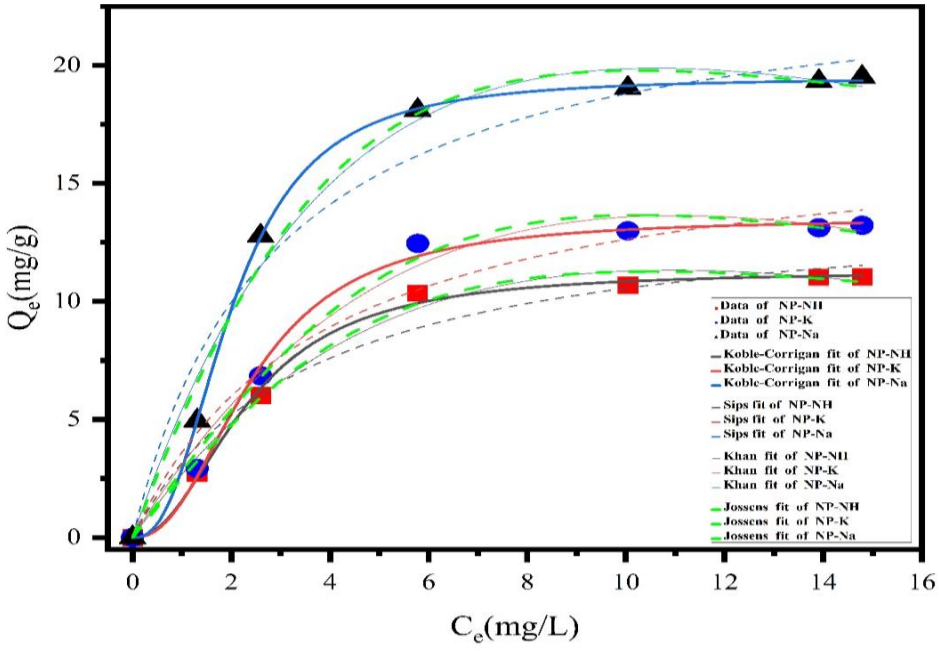

Figure 3a. Comparison of the isotherms of Sips, Koble-Corrigan, Khan, Jossens with the experimental data of NP-Na, NP-K and NP-NH.

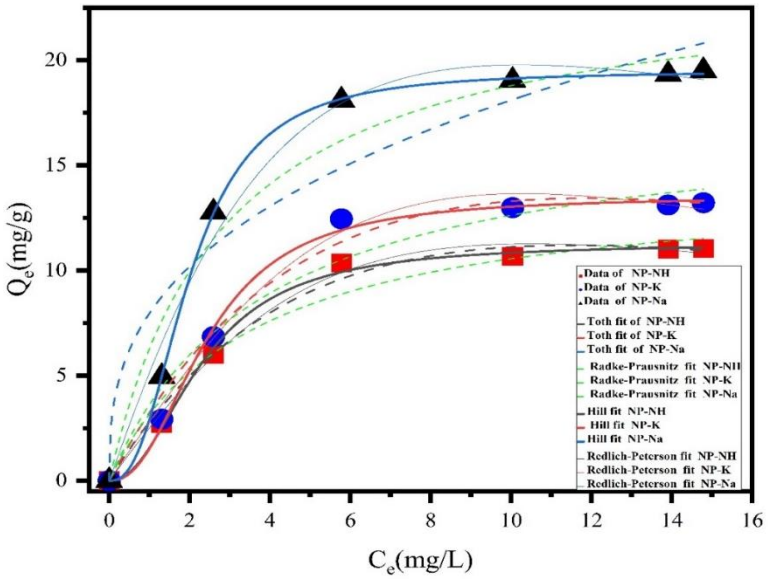

Figure 3b. Comparison of the isotherms of Redlich-Peterson, Radke-Prausnitz, Toth, and Hill with the experimental data of NP-Na, NP-K and NP-NH.

Table 3. Parameters for trace metals sorption isotherms fitted with of Koble-Corrigan, Redlich-Peterson, Jossens, Radke-Prausnitz, Khan, Toth, Sips and Hill for the samples NP-Na, NP-K and NP-NH.

Models	Parameters	Cadmium (Cd)		
		NP-NH	NP-K	NP-Na
Redlich-Peterson	K_R (L/g)	2.57161	2.83987	5.37504
	a_R (L/mg)	0.02473	0.0143	0.04711
	g	1.71543	1.87819	1.56187
	R^2	0.99317	0.99234	0.97109
	Reduced Chi-square (χ^2)	0.21232	0.35431	1.21796
	Adj. R^2	0.98975	0.98851	0.98064
	RSS	0.84928	1.41724	4.87183
Toth	(mg/g)q_m	38.08471	51.10463	59.31554
	(L/mg)K_T	0.11579	0.1043	0.14151
	t	1.71401	1.87575	1.56092
	R^2	0.99317	0.99234	0.98709
	Reduced Chi-square (χ^2)	0.21232	0.3543	1.21795
	Adj. R^2	0.98976	0.98851	0.98064
	RSS	0.84927	1.41721	4.8718
Hill	(mg/g)q_{SH}	11.929988	13.53089	19.48838
	K_H (L/g)	6.22934	7.86421	5.68571
	n_H	2.16907	2.31553	2.48439
	R^2	0.99723	0.99672	0.99989
	Reduced Chi-square (χ^2)	0.08624	0.15159	0.01008
	Adj. R^2	0.99584	0.99508	0.99984
	RSS	0.34497	0.60635	0.04032

Conclusion

The adsorption isotherm data of three different iron oxide nanomaterials for cadmium removal were fitted to isotherm models using non-linear regression methods. The results demonstrated that the Hill isotherm model best describes the experimental values of our adsorption isotherm study, indicating

that cadmium adsorption on magnetic iron oxides is a cooperative phenomenon, with adsorbates having the ability to bind to a site. Notably, the NP-Na sample exhibited the highest heavy metal removal capacity (19.36 mg/g) compared to NP-K (13.31 mg/g) and NP-NH (11.04 mg/g), despite having the lowest magnetization strength. This superior performance is attributed to the higher surface area and the presence of more micropores and mesopores in the NP-Na sample, which provide favorable conditions for adsorption. Additionally, the study confirmed that the removal efficiency is strongly dependent on the particle size, with smaller particles showing less aggregation and more active sites for adsorption. This study highlights the importance of selecting the appropriate isotherm model for a better understanding and optimization of adsorption processes, which is crucial for the development of effective heavy metal decontamination technologies.

Disclosure statement: *Conflict of Interest:* The authors declare that there are no conflicts of interest.
Compliance with Ethical Standards: This article does not contain any studies involving human or animal subjects.

References

Al-Ghouti M.A., Da'ana D.A. (2020). Guidelines for the use and interpretation of adsorption isotherm models: A review. *Journal of Hazardous Materials*, 393, 122383. https://doi.org/10.1016/j.jhazmat.2020.122383

Alshahateet, S.F., Al-Trawneh, S.A., Er-rajy, M., Zerrouk, M., Azzaoui, K., Al-Tawarh, W.M., *et al.* (2024) Green Synthesis of Zinc Oxide Nanoparticles for Tetracycline Adsorption: Experimental Insights and DFT Study. *Plants*, 13, 3386. https://doi.org/10.3390/plants13233386

Ayawei, N., Ebelegi, A. N., & Wankasi, D. (2017). Modelling and Interpretation of Adsorption Isotherms. *Journal of Chemistry*, 2017(1), 3039817. https://doi.org/10.1155/2017/3039817

Ayawei, N., Ebelegi, A. N., & Wankasi, D. (2017). Modelling and Interpretation of Adsorption Isotherms. *Journal of Chemistry*, 2017(1), 3039817. https://doi.org/10.1155/2017/3039817

Ayawei, N., Jnr, M. H., & Spiff, I. (2005). Rhizophora mangle waste as adsorbent for metal ions removal from aqueous solution. ResearchGate. *European Journal of Scientific Research*, 9(1), 21

Azzaoui K., Jodeh S., Mejdoubi E., *et al.* (2023) Synthesis of hydroxyapatite /polyethylene glycol 6000 composites by novel dissolution/ precipitation method: Optimization of the Adsorption Process using a Factorial Design: DFT and Molecular Dynamic. *BCM Chemistry*, 17(1),150. doi: 10.1186/s13065-023-01061-7.

Calvert, J. G. (1990). Glossary of atmospheric chemistry terms (Recommendations 1990). *Pure and Applied Chemistry*, 62(11), 2167-2219. https://doi.org/10.1351/pac199062112167

Chen, F., Ilyas, N., Liu, X., Li, Z., Yan, S., & Fu, H. (2021). Size Effect of Fe_3O_4 Nanoparticles on Magnetism and Dispersion Stability of Magnetic Nanofluid. *Frontiers in Energy Research*, 9. https://doi.org/10.3389/fenrg.2021.780008

Chowdhury, P., Athapaththu S., *et al.* (2017). Visible-solar-light-driven photo-reduction and removal of cadmium ion with Eosin Y-sensitized TiO_2 in aqueous solution of triethanolamine. *Separation and Purification Technology*, 174, 109-115. https://doi.org/10.1016/j.seppur.2016.10.011

Chu, K.H., Hashim, M.A., Debord, J., *et al.* (2023). The Jovanović adsorption isotherm in water contaminant research: Unmasking spurious versions and spotlighting the real thing. *Chemical Engineering Science*, 281, 119127. https://doi.org/10.1016/j.ces.2023.119127

El Hammari L., Latifi S., Saoiabi S., Saoiabi A., Azzaoui K., Hammouti B., Chetouani A., Sabbahi R. (2022), Toxic heavy metals removal from river water using a porous phospho-calcic hydroxyapatite, *Mor. J. Chem.* 10(1), 62-72, https://doi.org/10.48317/IMIST.PRSM/morjchem-v10i1.31752

Eze, S. O., Igwe, J. C., & Dipo, D. (2013). Effect of particle size on adsorption of heavy metals using chemically modified and unmodified fluted pumpkin and broad-leafed pumpkin pods. *International Journal of Biological and Chemical Sciences*, 7(2), 852-860. https://doi.org/10.4314/ijbcs.v7i2.40

Faust, S. D., & Aly, O. M. (2013). Adsorption Processes for Water Treatment. Elsevier

Guo, X., & Wang, J. (2019). Comparison of linearization methods for modeling the Langmuir adsorption isotherm. *Journal of Molecular Liquids*, 296, 111850. https://doi.org/10.1016/j.molliq.2019.111850

Hashem, A., Taha, G. M., Fletcher, A. J., Mohamed, L. A., & Samaha, S. H. (2021). Highly Efficient Adsorption of Cd (II) onto Carboxylated Camelthorn Biomass: Applicability of Three-Parameter Isotherm Models, Kinetics, and Mechanism. *Journal of Polymers and the Environment*, 29(5), 1630-1642. https://doi.org/10.1007/s10924-020-01991-6

Kazantzis, G., & Blanks, R. (1992). A mortality study of cadmium exposed workers. Edited proceedings of the seventh international cadmium conference, New Orleans, LA, 6-7 April 1992., 150-157. https://cir.nii.ac.jp/crid/1571135649331179008

Kolhatkar, A. G., Jamison, A. C., Litvinov, D., Willson, R. C., & Lee, T. R. (2013). Tuning the Magnetic Properties of Nanoparticles. *International Journal of Molecular Sciences*, 14(8), 15977-16009. https://doi.org/10.3390/ijms140815977

Liosis, C., Papadopoulou, A., Karvelas, E., Karakasidis, T. E., & Sarris, I. E. (2021). Heavy Metal Adsorption Using Magnetic Nanoparticles for Water Purification: A Critical Review. *Materials*, 14(24), 7500. https://doi.org/10.3390/ma14247500

Moro, K., Ello, A. S., Koffi, K. R., & Eroi, N. S. (2023). Mixed Maghemite/Hematite Iron Oxide Nanoparticles Synthesis for Lead and Arsenic Removal from Aqueous Solution. *Journal of Nanomaterials*, 2023(1), 8216889. https://doi.org/10.1155/2023/8216889

Moro, K., Ello, A. S., Meledge, D. E. J.-C., & Koffi, K. R. (2022). Synthesis of Magnetic Iron Oxide Fe_3O_4/α-Fe_2O_3 for the Adsorptive Removal of Cadmium from Aqueous Solution. *Chemical Science International Journal*, 31(2), 35-43. https://hal.science/hal-05198108

N'diaye, A., Kankou, M.S.A., *et al.* (2022). A review of biomaterial as an adsorbent: From the bibliometric literature review, the definition of dyes and adsorbent, the adsorption phenomena and isotherm models, factors affecting the adsorption process, to the use of typha species waste as adsorbent. *Communications in Science and Technology*, 7(2), 140-153. https://doi.org/10.21924/cst.7.2.2022.977

Ocampo-Pérez, R., Leyva-Ramos, R., Sanchez-Polo, M., & Rivera-Utrilla, J. (2013). Role of pore volume and surface diffusion in the adsorption of aromatic compounds on activated carbon. *Adsorption*, 19(5), 945-957. https://doi.org/10.1007/s10450-013-9502-y

Sivarajasekar, N., & Baskar, R. (2014). Adsorption of basic red 9 onto activated carbon derived from immature cotton seeds: Isotherm studies and error analysis. *Desalination and Water Treatment*, 52(40), 7743-7765. https://doi.org/10.1080/19443994.2013.834518

Smolensky, E. D., Park, H.-Y. E., Zhou, Y., Rolla, G. A., Marjańska, M., Botta, M., & Pierre, V. C. (2013). Scaling Laws at the Nano Size: The Effect of Particle Size and Shape on the Magnetism and Relaxivity of Iron Oxide Nanoparticle Contrast Agents. *Journal of materials chemistry. B, Materials for biology and medicine*, 1(22), 2818-2828. https://doi.org/10.1039/C3TB00369H

Thapa D., Palkar V.R., Kurup M.B., Malik S.K. (2004). Properties of magnetite nanoparticles synthesized through a novel chemical route. *Materials Letters*, 58(21), 2692-2694. https://doi.org/10.1016/j.matlet.2004.03.045

Varma, M. C., Kumar, A. M., Choudary, G. S. V. R. K., & Rao, K. H. (2012). Effect of particle size on saturation magnetization and magnetic anisotropy of $Ni_{0.65}Zn_{0.35}Fe_2O_4$ nanoparticles. *International Journal of Nanoscience*, 11(03), 1240003. https://doi.org/10.1142/S0219581X12400030

Walsh, K., Mayer, S., Rehmann, D., Hofmann, T., & Glas, K. (2020). Equilibrium data and its analysis with the Freundlich model in the adsorption of arsenic (V) on granular ferric hydroxide. *Separation and Purification Technology*, 243, 116704. https://doi.org/10.1016/j.seppur.2020.116704